# Eddy Current Flow Meter Measurements in liquid Sodium at high Temperatures

**Krauter, Nico**[1]
Helmholtz-Zentrum Dresden - Rossendorf (HZDR)
Bautzner Landstr. 400, D-01328 Dresden, Germany
n.krauter@hzdr.de

**Onea, Alexandru Aurelian**
Karlsruhe Institute of Technology (KIT)
Hermann-von-Helmholtz-Platz 1, D-76344 Eggenstein-Leopoldshafen, Germany
alexandru.onea@kit.edu

**Gerbeth, Gunter**
Helmholtz-Zentrum Dresden - Rossendorf (HZDR)
Bautzner Landstr. 400, D-01328 Dresden, Germany
g.gerbeth@hzdr.de

**Eckert, Sven**
Helmholtz-Zentrum Dresden - Rossendorf (HZDR)
Bautzner Landstr. 400, D-01328 Dresden, Germany
s.eckert@hzdr.de

[1] Corresponding author

## ABSTRACT

*We present measurement results for the flow rate of liquid sodium at temperatures up to 700 °C that were obtained with a high temperature prototype of an immersed Eddy Current Flow Meter. The experimental campaign was conducted at the SOLTEC-2 sodium loop at KIT. The main objective of the experiments is the high temperature qualification of the Eddy Current Flow Meter as part of the safety instrumentation of generation IV liquid metal cooled fast reactors. There it is intended to be used for monitoring the flow rate of the coolant and to detect possible blockages of sub assemblies. Due to the large liquid metal volume, the sensor has to be located close to the sub assemblies, therefore measurements from outside of the vessel are not possible and an immersed sensor is required. We demonstrate the successful application of the immersed Eddy Current Flow Meter at such high temperatures and identify the relevant effects with impact on the sensor performance.*


## INTRODUCTION

Measuring the flow rate in liquid metals is a challenging task due to their opacity, high corrosivity and melting temperatures that are typically in the order of several hundred degrees Celsius. Depending on the temperature, this results in considerable requirements for the deployed measurement equipment, especially for the selection of temperature-resistant materials which still allow for accurate measurements. Measurement techniques that are based on the ultrasound Doppler effect or the induction of eddy currents within the liquid metal have been successfully applied in the past for the measurement of the flow velocity, even at high temperatures, each with their own advantages and disadvantages [1-3]. While ultrasound Doppler velocimetry (UDV) enables the measurement of a complete velocity profile along the ultrasound beam, it is limited by the maximum operating temperature of the ultrasound transducer which is used to generate the ultrasound waves [4]. In addition, a good coupling between sensor and liquid metal is required for reliable measurements, which is especially difficult at higher temperatures. Usually UDV can be applied to liquid metal flows with temperatures up to 200 °C. By using acoustic wave guides, with a suitable design mode of appropriate materials the temperature range can be extended to 620 °C or even up to 900 °C, but this often comes at the price of a strongly reduced signal

strength [5]. Inductive measurement techniques have the advantage that there is no need for direct contact between sensor and the liquid metal [6,7]. They employ magnetic fields to generate eddy currents within the liquid metal, which depend on the electrical conductivity and, thus, the temperature of the metal, as well as on the flow velocity and can be detected by a suitable measurement setup. The measurement techniques that rely on permanent magnets to generate a magnetic field are limited by the Curie temperature of the permanent magnet [8,9]. Above this material-specific temperature, the magnet is losing its ferromagnetic properties and the sensor is no longer functional. For sensors where the magnetic field is generated by an electromagnet, the maximum operating temperature is typically only limited by the insulation material of the wire that is used for the construction of the coils. An inductive sensor of this kind is the Eddy Current Flow Meter (ECFM), which is used for the measurements that are presented in this paper.

The ECFM essentially consists of three coils, where the so-called primary coil is generating an alternating magnetic field and two passive secondary coils located ahead and behind the primary coil, which are used to detect changes in the magnetic field caused by the liquid metal flowing past the sensor. A more detailed description of the ECFM, its operating principle and recent experimental results for sodium flows can be found in [10-15].

## EXPERIMENTAL SETUP

### ECFM high-temperature prototype

The high-temperature ECFM sensor consists of three magnet coils on a MACOR coil holder with a diameter of 10.6 mm and a total length of 50 mm. MACOR is a special non-magnetic ceramic that is more easily machinable than conventional ceramics. The active primary coil is used for the generation of the excitation field and two passive secondary coils are used to detect velocity induced changes in the excitation field, which are produced by the liquid metal flowing around the sensor. The primary coil has a

height of 10 mm and 125 turns, the secondary coils each have a height of 16 mm and 250 turns (see Fig.1).

A special coil wire with the designation KD500 is used for the coils, it is a ceramic insulated, nickel plated copper wire with 27% nickel and a wire diameter of 0.25 mm. It is not recommended to use pure copper wire because the copper will oxidize at high temperatures. This corrosion increases exponentially with rising temperatures, which would result in a strongly reduced time of life for the ECFM sensor coils [16]. Using a nickel plated copper wire is a compromise between small wire resistance/diameter and high temperature corrosion resistance. By introducing nickel, the wire resistance is increased compared to using pure copper, which is an undesired effect. On the other hand, the nickel layer around the copper prevents corrosion at high temperatures while still having a comparably small wire diameter. Small wire diameters are important because they enable a higher number of coil windings, which increases the sensitivity of the sensor, for the limited space that is available. While the ceramic insulation makes the wire more susceptible to mechanical stress, it has the advantage of high temperature resistance and a thin insulating layer of only a few micrometres, keeping the overall diameter of the wire as small as possible. Other temperature-resistant insulations such as glass silk cannot be manufactured with such thin insulating layers, which would ultimately result in fewer turns for the coils and lower sensitivity of the sensor.

For the measurements, an excitation current with an RMS value between 200 mA to 500 mA and frequencies from 500 Hz to 2 kHz is applied to the primary coil of the sensor. Previous investigations with the ECFM in liquid sodium have shown that the sensor has its highest sensitivity in this frequency range, while increasing the current amplitude is directly increasing the sensitivity for the whole frequency range. Other factors that affect the sensitivity of the sensor include the wall thickness of the sensor casing, the volume of sodium around the sensor, the electrical conductivity of the sodium, and the distance of the sensor to other electrically conductive parts, such as the walls of the test section. The output voltage of the sensor is equal to the voltage

difference of the two secondary coils. This voltage is measured with a lock-in amplifier (LIA), which only takes voltages into account that have the same frequency as the excitation current of the ECFM and therefore strongly reduces the impact of electromagnetic noise on the measured signals. The sinusoidal excitation current with a constant rms is provided by a power amplifier, even if the resistance of the excitation coil changes due to fluctuations in temperature. The investigated sodium velocities in the annular gap between the inner pipe housing of the sensor and the outer pipe of the test section are between 0 m/s and 0.8 m/s.

**Experimental Facility**

The SOLTEC-2 liquid sodium loop [17] mainly consists of a low and a high temperature branch. The two branches are connected by a sodium-sodium heat recuperator which is directly coupled to a sodium-air heat exchanger. A third branch contains the connection to the argon system. The piping of the low temperature branch is manufactured from stainless steel and contains a permanent magnet pump with a total power of 3 kW. The high temperature branch contains a 6.3 kW high temperature heater which is able to heat the sodium to a maximum temperature of 720°C, which is the maximal specified operation temperature of the loop. To make the loop as compact as possible, the sodium storage tank is also used as an expansion tank.

A permanent magnet rotating pump with a standard motor as the primary drive is used to pump the liquid sodium through the loop. By varying the motor power $P_m$ of the primary drive, the flow rate of the sodium can be adjusted. The maximum specified sodium flow rate of the loop is 300 kg/h and the maximal overpressure is 3.5 bar. The low temperature branch is limited to temperatures below 450 °C, which is the maximal operating temperature of the sodium pump. The high temperature branch, which contains the test section can be operated with sodium temperatures up to 720 °C. The piping diagram of the loop and a schematic of the test section are presented in Fig. 2. The temperature of the loop is monitored with several thermocouples that are distributed throughout the different branches, there are also three pressure sensors and

a fly-wheel sodium flow meter, which is located close to the sodium pump in the low temperature branch of the loop.

At the SOLTEC-2 facility, the ECFM is placed in a specially designed test section in the high temperature branch of the loop. There are five thermocouples distributed throughout the test section in order to monitor the temperatures of the test section and the ECFM. Since thermocouple T3 is closest to the ECFM, its output is used as the reference temperature for the sensor, which is protected from direct contact with the liquid sodium by a stainless steel casing with a wall thickness of 2 mm and an inner diameter of 11 mm. For this configuration of test section and sensor, the gap between the outer pipe and the inner pipe housing of the ECFM has a width of 3 mm, sufficient enough not to cause blockages of the sodium flow. Due to the high temperatures, the heat-resistant austenitic chromium-nickel steel 1.4841 (X15CrNiSi25-21) is used as the material for the sensor casing. Since the gap width of 3 mm is much smaller than the penetration depth of the excitation field at 1 kHz into liquid sodium, which is about 6 mm depending on the sodium temperature, the sensitivity of the ECFM to velocity changes is reduced compared to previous experiments with the ECFM performed in [13-15].

**EXPERIMENTAL RESULTS**

The measurements with the ECFM were obtained over a period of two days. On the first day, the temperature was increased gradually up to 600 °C. Measurement data with varying flow rates were recorded at temperatures of 150 °C, 200 °C, 300 °C, 400 °C, 500 °C and 600 °C. On the second day, the loop was heated to 700 °C after performing some comparative measurements at 150 °C (see Fig. 3). Several effects were observed during the measurements, which will be presented in the following subsections. During the two days, the sensor was not moved in order to prevent effects that would result from a slightly different position or angle of the sensor. The sensor was not damaged during the measurement campaign and was fully operational at the end of the second day. Compared to other liquid metal coolants, the electrical conductivity of sodium

varies largely in the range between 150 °C ($8.9 \cdot 10^6$ $\Omega^{-1}m^{-1}$) and 700 °C ($2.6 \cdot 10^6$ $\Omega^{-1}m^{-1}$) [18]. This has an impact on the sensitivity of the ECFM, since the amplitude of the induced eddy currents within the liquid metal depends on its electrical conductivity. Therefore, the ECFM has to be calibrated for different temperatures with the help of other flow sensors in order to provide accurate measurement results for the flow velocity. In the present case, the flow rate data of the fly-wheel are used as a reference for the ECFM.

**Filling and draining of the loop**

Fig. 4 shows how the presence or absence of sodium changes the output voltage of the ECFM. Before $t$ = 38 s the test section is filled with liquid sodium at 267 °C. Shortly thereafter, a brief drop in the voltage indicates that the sensor detects a movement of the liquid metal, which is caused by the sodium being drained from the test section. Subsequently it can be seen that the sodium is completely drained from the test section at $t$ = 45 s, as the output voltage has increased significantly. The output voltage increases because without the sodium near the sensor, there are no induced eddy currents that would reduce the output voltage with their own magnetic field opposing the excitation field. A similar behavior of the output voltage can be observed during filling of the test section, although there are much stronger fluctuations of the sensor temperature, when the hot sodium enters the empty test section, which also increases the oscillations of the output voltage. This is caused by slight (undesirable) asymmetries in positioning and other geometrical or electrical parameters in the secondary coils. Due to manufacturing tolerances, a voltage offset occurs which is not determined by the flow velocity but by the electrical conductivity of the liquid metal. With an ideal, perfectly symmetrical coil arrangement it would not be possible to detect the presence or absence of the sodium by analyzing the voltage difference of the two secondary coils.

**Nickel migration**

The coils of the ECFM are made of nickel-plated copper wire with a 27 % nickel content, which prevents oxidation of the copper at high temperatures and at the same time allows for a relatively low wire resistance. Above temperatures of 315 °C, an effect called nickel migration occurs, in which nickel slowly permeates into the outer layers of the copper. This results in an increase of the wire resistance and is significant for wire diameters below or equal 0.15 mm. In order to investigate this effect for the coil wire with a wire diameter of 0.25 mm that was used for the construction of the high-temperature ECFM, a different ECFM sensor was placed in an oven and multiple temperature cycles between room temperature and 600 °C were performed prior to the experiments at the SOLTEC-2 loop. The resulting increase in wire resistance after each cycle can be seen in Fig. 5. An increased wire resistance of the secondary coils has a slight impact on the measured sensor output voltage caused by the increased wire resistance and the internal resistance of the LIA, although the effect of nickel migration is much smaller than the influence of temperature on the wire resistance. When comparing the wire resistance of the ECFM at room temperature before and after the experimental campaign, an increase of ca. 10% was observed.

**Curie temperature of the coil wire**

As described in the previous subsection, the coil wire contains nickel, which is a ferromagnetic metal. It has a similar effect on the coils as using a ferromagnetic core, which is increasing the inductivity and thus the strength of the magnetic field of a coil. Ferromagnetic materials, like nickel, lose their ferromagnetic properties above a specific temperature which is called the Curie temperature. For pure nickel this temperature is 354 °C and it is lower for copper-nickel alloys, depending on the nickel content. Above the Curie temperature, the inductivity of the ECFM coils is considerably reduced. This manifests itself in a reduced amplitude of the sensor output voltage but seems to have no or only a small impact on the velocity sensitivity of the sensor.

In Fig. 6 the magnitude of the sensor output voltage is displayed for heating and cooling around the Curie temperature. It can be seen, that the effects on the voltage are starting around 335 °C and last until 355 °C. Due to the positioning of thermocouple T3, there might be a minor temperature discrepancy between the measured temperature and the actual temperature of the sensor. The plateau around 345 °C suggests a temperature difference between the two secondary coils, which reach their Curie temperature at different temperatures of T3. This plateau can be observed for heating and cooling of the loop at both days of the measurement campaign. In order to better compare the two curves in Fig. 6, the orange curve was shifted by -2 °C and scaled, to match the blue curve. The temperature difference of 2 °C can be attributed to differences in the temperature distribution between thermocouple T3 and the actual ECFM temperature. The higher voltage during cooling is most likely caused by the wetting of the sensor casing after a certain time of the temperature increase above 300 °C, since it cannot be observed for heating and cooling at the second day. Due to the strong changes of the output voltage and the uncertainty whether both coils have reached their Curie temperature, the ECFM cannot provide reliable flow rate measurements in the temperature range between 330 °C and 360 °C when using this kind of wire. Although it can easily be determined which of the coils has reached its Curie temperature by measuring the inductivity or impedance of the coils. This would require additional measurement equipment and appears as not suitable for the limited temperature range between 330 °C and 360 °C.

**Wetting of the sensor casing**

The basic operation of the ECFM was tested at 150 °C on the first and second day of the measurement campaign by varying the motor power of the sodium pump between 4% and 12% while keeping the temperature as constant as possible. From the measurement results of the first day in Fig. 7 it can be seen that the ECFM output voltage changes according to the motor power. Some oscillations of the signal can be observed, as well as a signal difference of 10 µV at $P_m$ = 4% before and after cycling through the various $P_m$. Instead of the absolute voltage, the voltage change $\Delta V$ of the

sensor output is displayed, so that it is easier to compare the results at different temperatures, where the absolute voltage changes as a result of the increased wire resistance and reduced electrical conductivity of the liquid metal. The absolute voltage that is measured by the LIA is comprised of the velocity-dependent part $\Delta V$ and a part that does not depend on the velocity. This offset is caused by asymmetries in the geometry, position and electrical parameters of the secondary coils and is present even at zero velocity. Because this offset changes at different temperatures, $\Delta V$ is displayed instead of the total output voltage. Since the real part of the output voltage has a higher sensitivity at 150 °C than the magnitude, it is used here instead to better demonstrate the influence of the wetting of the sensor casing.

The measurements at 150 °C were repeated on the second day of the measurement campaign. The output voltage of the ECFM is displayed in Fig. 8 together with the motor power and the flow rate that was measured with the fly-wheel. A change of 1% of motor power corresponds to a flow rate change of 0.012 l/s or 0.05 m/s.

The fly-wheel takes a few minutes after a change of motor power to display the actual flow rate, while the ECFM is reacting to flow rate changes almost instantaneously. Compared to the measurements of the first day, the oscillations on the voltage signal are considerably lower, the overall sensitivity to changes in the flow rate is increased by ca. 30% and the signal difference that was observed on the first day after returning to the lowest flow rate has vanished. These effects are most likely due to the wetting of the sensor casing during the first day of the measurement campaign. Typically, wetting of sodium on stainless steel begins when the temperature exceeds 300 °C for an extended period of time and provides a better contact between sensor casing and liquid metal. As can be seen from the results, wetting of the sensor casing has several beneficial effects on flow rate measurements with the ECFM.

From the steady-state flowrate of the flywheel and the cross section area of the annular channel around the ECFM, where the liquid sodium flows, the ECFM can be calibrated such that the flow velocity within the channel can be calculated directly from

the ECFM output voltage. When using the measurement data for $T$ = 150 °C of the second day, the calibration equation $v$ (m/s) = $-3.4473 \cdot 10^{-3} \cdot V_{real}$ (V) + 11.584 is obtained. The resulting flow velocities are plotted in Fig. 9. Once the ECFM is calibrated for a given temperature, the Na flow velocities inside the test section can be obtained almost instantly without the time delay of a few minutes as it is characteristic for the fly-wheel. These steps demonstrate the general approach for calibrating the ECFM for a constant liquid metal temperature. Depending on the application, it may be necessary to calibrate the ECFM for different temperature ranges. From the data that were obtained in this measurement campaign, it would be possible to calibrate the ECFM for the complete operating range of the SOLTEC facility of 150 °C to 700°C. On the other hand, this demonstrates a disadvantage of the ECFM, namely the need for a second flow rate sensor which is essential for the initial calibration of the ECFM.

**ECFM sensitivity at different temperatures**

The sensitivity of the ECFM is an indicator of how much the output voltage changes for a corresponding variation in flow rate or in this case for a change in the motor power $P_m$. It is determined by calculating the mean voltage for each investigated $P_m$ at a constant temperature and subsequently performing a linear regression of these values. The slope of the resulting linear function is the sensitivity of the ECFM with the unit µV per % motor power and shown in Fig. 10.

The values at 600 °C and 700 °C must be taken with caution since only two different flow rates or data points were used for the linear regression, which is the minimum amount, possibly with a certain margin of error. Unfortunately, only two different flow rates could be selected at high temperatures. Otherwise, the temperature would drop considerably if the flow rate is too high (see Fig. 3 at 14:30 on the 2nd day) or the sodium will flow back into the storage tank if the flow rate is too low. Additionally, a strong influence of the temperature on the output voltage was observed for temperatures above 500 °C, due to the increased wire resistance at high temperatures.

Most measurements were performed for an excitation current of 200 mA rms and a frequency of 1 kHz. Additional measurements were performed with an increased rms of 500 mA and frequencies of 500 Hz and 2 kHz to determine how it affects the sensitivity of the sensor. An overview of the sensitivity of the sensor regarding real part, imaginary part, magnitude and phase shift of the output voltage is given in Fig. 10. At lower temperatures, real part and phase shift provide the best results with the highest sensitivities, which is gradually decreasing for higher temperatures to almost zero at 500 °C and 600 °C. The overall best results over a wide range of temperatures is provided by the voltage magnitude. Increasing the rms of the excitation current increases the sensitivity in general, the best results at high temperatures were achieved at a frequency of 2 kHz. Due to the strong change of electrical conductivity of sodium between 150 °C and 700 °C, there is no single optimal frequency. According to numerical simulations, the optimal frequency is shifted to higher frequencies with increasing temperatures and for the phase shift, the sensitivity is strongly reduced at high sodium temperatures or low electrical conductivities [19]. This is in good agreement with the results that were obtained in the experimental campaign.

Especially around temperatures of 700 °C, which is the highest investigated temperature, the increased wire resistance results in a strong influence of temperature fluctuations on the output voltage of the ECFM. The effect on the output voltage is demonstrated in Fig. 11, where the velocity and temperature dependent changes of the output voltage are displayed. In this example, a temperature difference of 7 °C at a constant flow rate corresponds to a change of 10 µV of the output voltage while a 1 % change in motor power (≈ 0.05 m/s) at a constant temperature results in an output difference of 25 µV. It can be seen that temperature fluctuations can have a significant influence on the output voltage, especially for small velocity changes. If temperature and velocity vary simultaneously, it is not clear which part of the total output voltage can be attributed to each of these parameters without monitoring the temperature. Although this effect is negligible at low temperatures or large changes in flow velocity, it has to be considered above a certain operating temperature, depending on the desired

measurement accuracy and for how many temperature levels the ECFM has been calibrated. By monitoring the temperature and/or increasing the excitation current such that the sensitivity to velocity fluctuations is greater than the sensitivity to temperature changes, the negative effects can be mitigated but it might not be possible to resolve very small velocity changes.

Since the volume of sodium around the sensor with a gap width of 3 mm is relatively small at the test section, the sensitivity to velocity changes is much smaller than in pool type flows. While the sensitivity to temperature fluctuations is not influenced by the sodium volume around the sensor, the velocity sensitivity can be significantly increased by increasing the liquid metal volume up to three times the penetration depth. Therefore, a much smaller influence of the temperature on the output voltage of the ECFM at similar temperatures is expected in applications with large sodium volumes which are typically the case in liquid metal cooled fast reactors. For example, the normal operating temperature in the ASTRID 600 sodium cooled fast reactor lies between 400 °C and 550 °C [20] with flow velocities up to 3 m/s [21]. As the flow velocities in the reactor are expected to be three times higher than in the experiments, the signal strength of the ECFM will also increase by a factor of 3, as it depends linearly on the flow velocity of the liquid metal, which leads to more stable measurement results. Regarding the temperature, it was demonstrated that the sensor can operate at 700 °C and is designed to withstand even higher temperatures.

**Measurement errors**

When performing the linear regression for the calculation of the sensitivity of the ECFM, the data points usually do not fit perfectly to the calculated linear function of voltage versus motor power or flow velocity. In order to be able to estimate the measurement error of the sensitivity of the ECFM, which is an indicator for how accurate the calibration of the ECFM has been performed, the standard deviation can be calculated. When comparing the relative standard deviation $s_{rel}$ for real part, imaginary

part, magnitude and phase of the ECFM output voltage in Tab. 1, it can be seen that the real part provides the lowest measurement error in most cases.

Unfortunately, $s_{rel}$ cannot be calculated for the measurements with $T \geq 600$ °C because the number of different flow rates was limited to two realizations. The linear regression of two data points always results in a standard deviation of zero which does not represent a real estimate for the quality of the sensor calibration. In general, the calibration of the ECFM should be performed with as many data points as possible in order to increase the reliability of the calibration equation. The fly-wheel sensor introduces an additional measurement error of ±1.5% of the steady-state value. A detailed investigation of a similar sensor can be found in [22]. K-type thermocouples with a measurement accuracy of ±1.5 °C were used for the temperature measurements. The thermocouple data logger introduces an additional error of ± 0.2% of the indicated temperature ±0.5 °C. In the worst case, according to error propagation this would result in a total absolute measurement uncertainty of ±2.1 °C for a measured temperature of 700 °C.

## CONCLUSIONS

A high-temperature prototype of the ECFM, which was developed at HZDR, was successfully tested in liquid sodium with temperatures up to 700 °C at the SOLTEC-2 facility at KIT. This flow rate sensor consists of temperature resistant materials that enable its use in liquid metal cooled fast reactors for monitoring the coolant flow. During the measurement campaign with a duration of two days, the sensor was operating as intended, and changes of the flow rate could be detected at all investigated temperatures up to 700 °C. The measurements became more difficult at the highest investigated temperatures because of several effects: due to nickel migration and increasing temperatures, the wire resistance of the sensor coils increases, which has a negative impact on the quality of the output voltage by adding additional fluctuations on the velocity dependent part of the voltage which are caused by changes in temperature. With rising temperatures, the influence of the temperature on the output

voltage also increases. Since the coil wire contains nickel, the sensor cannot be used reliably between 330 °C and 360 °C due to the Curie temperature, where the coils abruptly lose some portion of their inductivity. This has a strong impact on the output voltage but no significant impact on the sensitivity, at least for this measurement setup where the sensor is surrounded by a relatively small volume of sodium. The positive effect of wetting of the stainless steel sensor casing was also observed. As demonstrated, the sensitivity of the sensor can be increased by changing the excitation frequency and/or increasing the RMS of the excitation current.

The viability of the ECFM sensor for deployment at high liquid metal temperatures has been demonstrated. For the further qualification of the ECFM, a different test mock-up can be envisaged, where a larger sodium volume and larger flow rates can be considered for a comprehensive investigation of the sensor at high temperatures and a better approximation of the flow conditions inside a reactor. Another challenging task is the development of some type of temperature compensation for the output voltage of the sensor, since the influence of the temperature on the signals, especially at high temperatures, is considerable and results in a reduction of measurement accuracy for the flow rate measurements.

**ACKNOWLEDGMENT**

The authors would gratefully thank Uwe Häfner, Oliver Albrecht and Rupert Schmidt, who assisted with the construction of the test section and the measurement setup.

**FUNDING**

Results presented here have received funding from the Euratom research and training programme 2014-2018 in frame of the project ESFR-SMART under the grant agreement No. 754501.

## NOMENCLATURE

| | |
|---|---|
| $P_m$ | motor power of the primary drive for the permanent magnet pump, % |
| $R_P$ | electrical resistance of the coil wire of the primary coil, Ω |
| $s_{rel}$ | Relative standard deviation, % |
| $t$ | time, s |
| $T$ | temperature, °C |
| $u_{fw}$ | flow rate indicated by the fly wheel, l/s |
| $v$ | flow velocity of the liquid sodium, m/s |
| $V_{imag}$ | imaginary part of the sensor output voltage, V |
| $V_{mag}$ | magnitude of the sensor output voltage, V |
| $V_{real}$ | real part of the sensor output voltage, V |

### Greek Letters

| | |
|---|---|
| $\Delta P$ | difference in motor power $P_m$, % |
| $\Delta T$ | difference in temperature, °C |
| $\Delta V$ | voltage difference, V |
| $\Delta V_{real}$ | voltage difference (real part), V |
| ϕ | phase shift of the sensor output voltage, ° |

### Subscripts or Superscripts

| | |
|---|---|
| c | cooling |
| fw | flywheel |
| h | heating |
| m | motor |
| mag, real, imag | magnitude, real part, imaginary part |
| p | primary coil |
| rel | relative |

### Acronyms and abbreviations widely used in text and list of references

| | |
|---|---|
| ECFM | eddy current flow meter |
| KD500 | designation of coil wire used for the construction of the sensor |
| LIA | lock-in amplifier |
| MACOR | an easily machinable glass-ceramic |
| Na | sodium |
| RMS | root mean square |
| SOLTEC | SOdium Loop for TEst materials and Corrosion facilities |

| | |
|---|---|
| T1, T2, T3, T4, T5 | designation of the thermocouples distributed throughout the test section |
| UDV | ultrasound Doppler velocimetry |

**REFERENCES**

[1] Eckert, S., Buchenau, D., Gerbeth, G., Stefani, S., Weiss, F. P., 2012, "Some Recent Developments in the Field of Measuring Techniques and Instrumentation for Liquid Metal Flows," Journal of Nuclear Science and Technology, **48**(4), pp. 490-498. DOI: 10.1080/18811248.2011.9711724

[2] Rajan, K. K., Jayakumar, T., Aggarwal, P. K., Vinod, V., 2016, "Sodium flow measurement in large pipelines of sodium cooled fast breeder reactors with bypass type flow meters," Annals of Nuclear Energy, **87**(2), pp. 74-80. DOI: 10.1016/j.anucene.2015.08.018

[3] Ratajczak, M., Hernández, D., Richter, T., Otte, D., Buchenau, D., Krauter, N., Wondrak, T., 2017, "Measurement techniques for liquid metals," IOP Conference Series-Materials Science and Engineering, **228**, 012023. DOI: 10.1088/1757-899X/228/1/012023

[4] Eckert, S., Gerbeth, G., 2002, "Velocity measurements in liquid sodium by means of ultrasound Doppler velocimetry," Experiments in Fluids, **32**(5), pp. 542-546. DOI: 10.1007/s00348-001-0380-9

[5] Eckert, S., Gerbeth, G., Melnikov, V.I., 2003, "Velocity measurements at high temperatures by ultrasound Doppler velocimetry using an acoustic wave guide," Experiments in Fluids, **35**, pp. 381–388. DOI: 10.1007/s00348-003-0606-0

[6] Priede, J., Buchenau, D., Gerbeth, G., 2011, "Contactless Electromagnetic Phase-Shift Flowmeter for Liquid Metals," Measurement Science and Technology, **22**, 055402. DOI: 10.1088/0957-0233/22/5/055402

[7] Stefani, F., Gundrum, T., Gerbeth, G., 2004, "Contactless inductive flow tomography," Physical Review E, **70**(5), 056306. DOI: 10.1103/PhysRevE.70.056306

[8] Rajan, K. K., Sharma, V., Vijayakumar, G., Jayakumar, T., 2015, "Design and development of samarium cobalt based permanent magnet flow meter for 100NB pipe in sodium circuits," Annals of Nuclear Energy, **76**, pp. 357-366. DOI: 10.1016/j.anucene.2014.10.007

[9] Priede, J., Buchenau, D., and Gerbeth, G., 2011, "Single-magnet rotary flowmeter for liquid metals," Journal of Applied Physics, **110**(3), 034512. DOI: 10.1063/1.3610440

[10] Sureshkumar, S., Sabih, M., Narmadha, S., Ravichandran, N., Dhanasekharan, R., Meikandamurthy, C., Padmakumar, G., Vijayashree, R., Prakash, V., Rajan, K.K., 2013, "Utilization of eddy current flow meter for sodium flow measurement in FBRs," Nuclear Engineering and Design, **265**, pp. 1223– 1231. DOI: 10.1016/j.nucengdes.2013.07.016

[11] Wiegand, D. E., Michels, C. W., 1969, "Performance tests on an eddy-current flowmeter," IEEE Transactions on Nuclear Science, **16**(1), pp. 192-195. DOI: 10.1109/TNS.1969.4325106

[12] Pavlinov, A., Khalilov, R., Mamikyn, A., Kolesnichenko, I., 2017, "Eddy current flowmeter for sodium flow," IOP Conference Series-Materials Science and Engineering, **208**, 012031. DOI: 10.1088/1757-899X/208/1/012031

[13] Krauter, N., Franke, S., Gerbeth, G., Eckert, S., Stefani, F., Gastaldi, O., Girard, M., 2018, "Eddy current flowrate and local ultrasonic velocity measurements in liquid sodium," Fast Reactors and Related Fuel Cycles: Next Generation Nuclear Systems for Sustainable Development (FR17) Proceedings Series, CN245-535.

[14] Krauter, N., Galindo, V., Wondrak, T., Eckert, S., Gerbeth, G., 2021, "Eddy Current Flow Meter Performance in Liquid Metal Flows Inclined to the Sensor Axis," ASME Journal of Nuclear Engineering and Radiation Science, **8**(1), 011303. DOI: 10.1115/1.4050420

[15] Krauter, N., Eckert, S., Gerbeth, G., 2023, "Coolant flow monitoring with an eddy current flow meter at a mock-up of a liquid metal cooled fast reactor," [Manuscript submitted for publication], Fast Reactors and Related Fuel Cycles: Sustainable Clean Energy for the Future (FR22) Proceedings Series, CN291-12.

[16] Wan, Y., Wang, X., Sun, H., Li, Y., Zhang, K., Wu, Y., 2012, "Corrosion Behavior of Copper at Elevated Temperature," International Journal of Electrochemical Science, **7**, pp. 7902-7914. Free download from https://www.researchgate.net/publication/266870651_Corrosion_Behavior_of_Copper_at_Elevated_Temperature

[17] Onea, A., Hering, W., Reiser, J., Weisenburger, A., Diez de los Rios Ramos, N., Lux, M., Ziegler, R., Baumgärtner, S., Stieglitz, R., 2017, "Development of high temperature liquid metal test facilities for qualification of materials and investigations of thermoelectrical modules," IOP Conference Series-Materials Science and Engineering, **228**, 012015. DOI: 10.1088/1757-899X/228/1/012015

[18] Sobolev, V., 2011, "Database of thermophysical properties of liquid metal coolants for GEN-IV," BLG Open Report Series of the Belgian Nuclear Research Centre, Mol (Belgium), ISSN: 1379-2407, Free download from https://inis.iaea.org/collection/NCLCollectionStore/_Public/43/095/43095088.pdf

[19] Krauter, N., 2019, *Entwicklung induktiver Strömungs- und Füllstandssensoren für flüssige Metalle*, TUDpress, Dresden, Germany, 250 pages, ISBN: 978-3-95-908165-8

[20] Jadot, F., Baqué, F., Jeannot, J. P., de Dinechin, G., Augem, J. M., Sibilo, J., 2011, "ASTRID sodium cooled fast reactor: Program for improving in service inspection and repair," 2nd International Conference on Advancements in Nuclear Instrumentation, Measurement Methods and their Applications. DOI: 10.1109/ANIMMA.2011.6172910

[21] Takano, K., Ohki, S., Ozawa, T., Yamano, H., Kubo, S., Ogura, M., Yamada, Y., Koyama, K., Kurita, K., Costes, L., Venard, C., Carluec, B., Perrin, B., Verrier, D., 2022, "Core and safety design for France–Japan common concept on sodium-cooled fast reactor," EPJ Nuclear Sci. Technol. **8**(35). DOI: 10.1051/epjn/2022040

[22] Hvasta, M. G., Dudt, D., Fisher, A. E., Koleman, E., 2018, " Calibrationless rotating Lorentz-force flowmeters for low flow rate applications," Meas. Sci. Technol., **29**, 075303. DOI: 10.1088/1361-6501/aac3b5

**Figure Captions List**

Fig. 1 Dimensions of the ECFM coil holder (mm), b) photograph of the sensor and a scheme of the coil arrangement for the primary and secondary coils

Fig. 2 a) Simplified piping diagram and b) scheme (not to scale) of the test section in the high temperature branch of the loop and position of the thermocouples T1-T5

Fig. 3 Temperature profile of the ECFM (thermocouple T3) during the two-day measurement campaign

Fig. 4 Voltage magnitude and temperature of the ECFM during draining of the loop, beginning at $t$ = 38 s

Fig. 5 Resistance of the primary coil of a different ECFM for three heating/cooling cycles between 20°C and 600 °C in an oven, conducted before the measurement campaign

Fig. 6 Magnitude of the ECFM output voltage as a function of the ECFM temperature during heating $V_{mag,h}$ and cooling $V_{mag,c}$ of the loop between 320 °C and 360 °C

Fig. 7 Real part of the ECFM output voltage for motor powers between 4% and 12 % at 150 °C on the first day of the measurement campaign

Fig. 8 Real part of the ECFM output voltage for motor powers between 4% and 12 % and the flow rate output $u_{fw}$ of the fly-wheel at 150 °C on the second day of the measurement campaign

Fig. 9 Flow velocities at 150 °C on the second day of the measurement campaign when applying the calibration equation to the real part of the ECFM output voltage

Fig. 10 Sensitivity of real part, imaginary part, magnitude and phase of the ECFM output voltage for different temperatures at both days of the measurement campaign. Data points without a separate description were

recorded with an excitation current of 200 mA rms and a frequency of 1 kHz

Fig. 11 Influence of temperature and motor power changes on the ECFM output signal at Na temperatures around 700 °C and an excitation current of 500 mA at 1 kHz, for a constant temperature with varying motor power a) and varying temperatures with a constant motor power b)

**Table Caption List**

Table 1 Relative standard deviations $s_{rel}$ for the determined sensitivities with an excitation current of 200 mA and 1 kHz

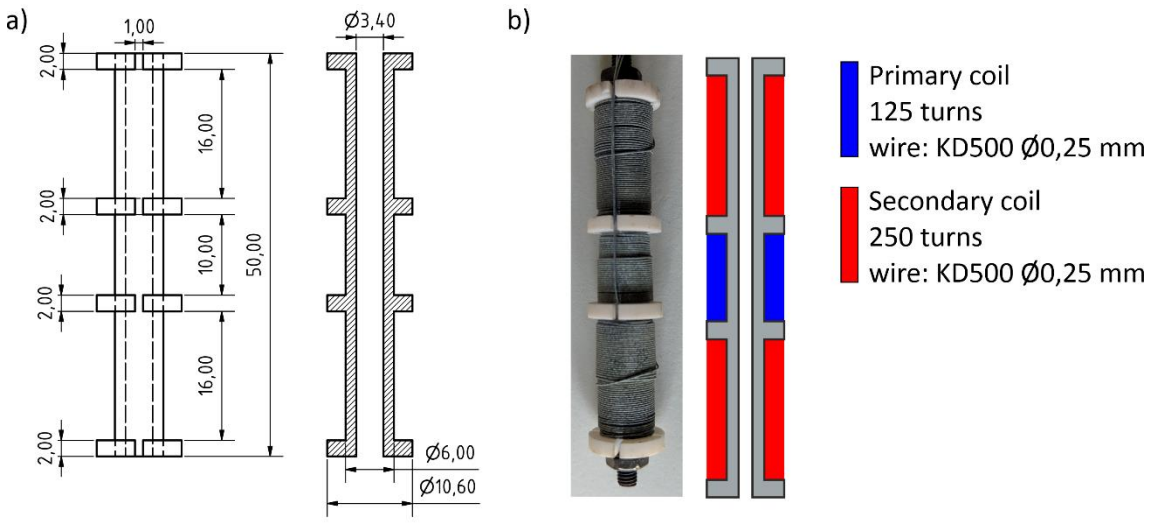
a)
1,00
Ø3,40
2,00
16,00
2,00
10,00
50,00
2,00
16,00
2,00
Ø6,00
Ø10,60
b)
Primary coil
125 turns
wire: KD500 Ø0,25 mm
Secondary coil
250 turns
wire: KD500 Ø0,25 mm

Fig. 1

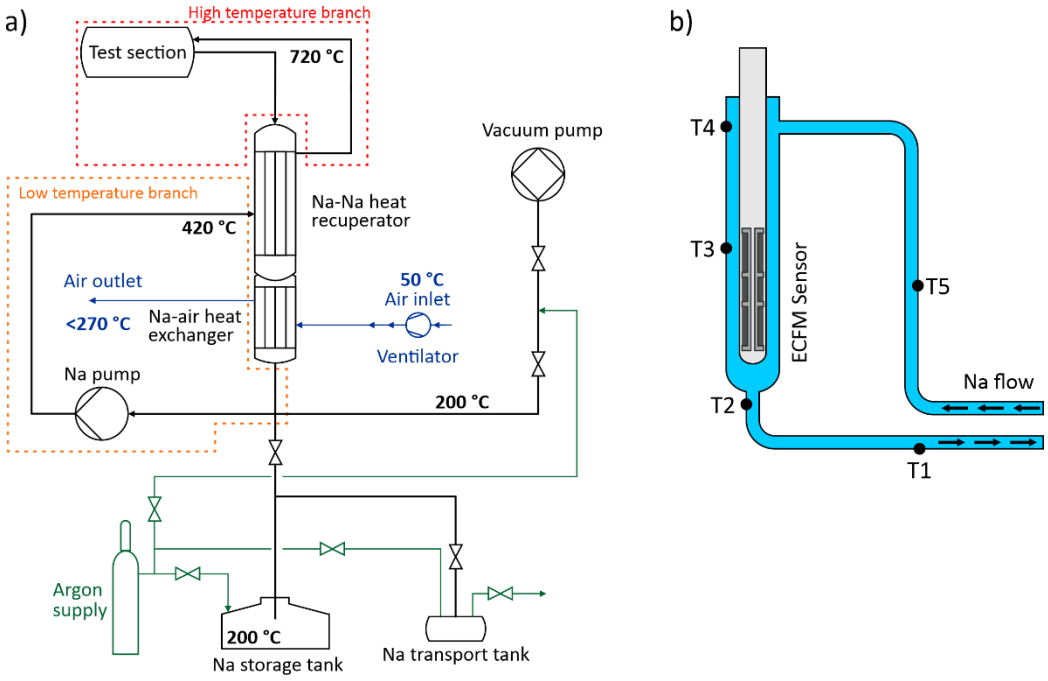
a)
High temperature branch
Test section
720 °C
Vacuum pump
Low temperature branch
420 °C
Na-Na heat recuperator
Air outlet
<270 °C
Na-air heat exchanger
50 °C
Air inlet
Ventilator
Na pump
200 °C
Argon supply
200 °C
Na storage tank
Na transport tank
b)
T4
T3
ECFM Sensor
T5
Na flow
T2
T1

Fig. 2

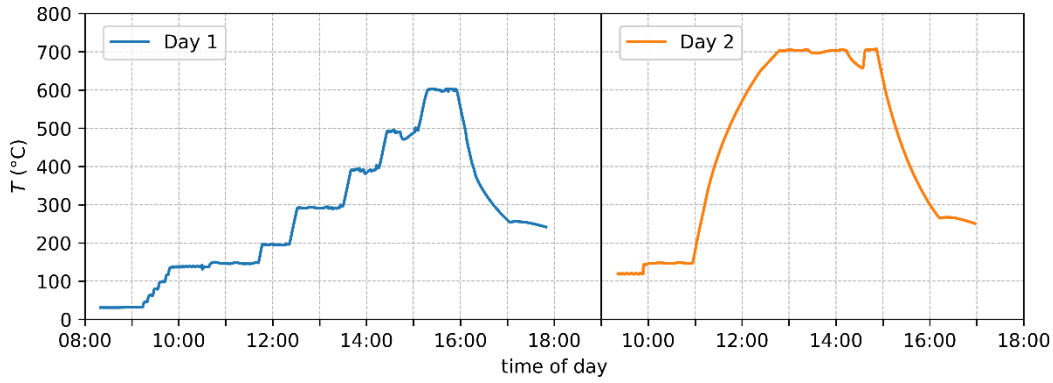
Day 1
Day 2
T (°C)
800
700
600
500
400
300
200
100
0
08:00
10:00
12:00
14:00
16:00
18:00
10:00
12:00
14:00
16:00
18:00
time of day

Fig. 3

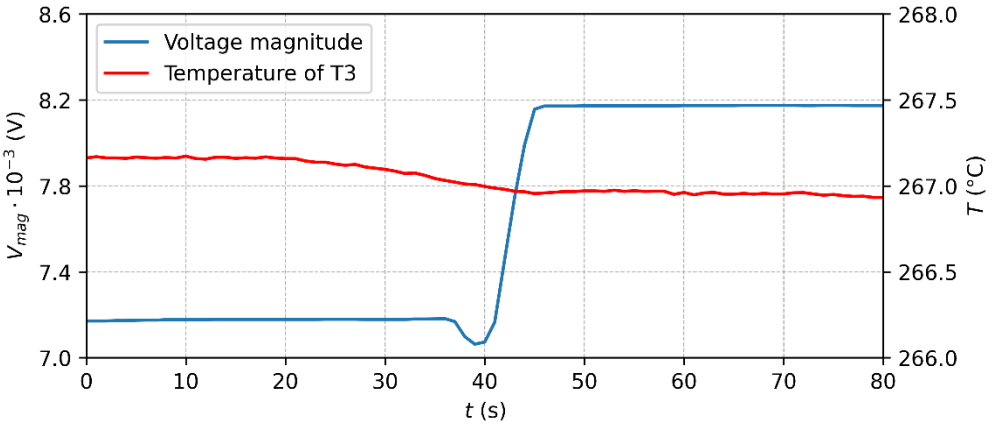
Voltage magnitude
Temperature of T3
8.6
8.2
7.8
7.4
7.0
$V_{mag}$, $10^{-3}$ (V)
268.0
267.5
267.0
266.5
266.0
$T$ (°C)
0
10
20
30
40
50
60
70
80
$t$ (s)

Fig. 4

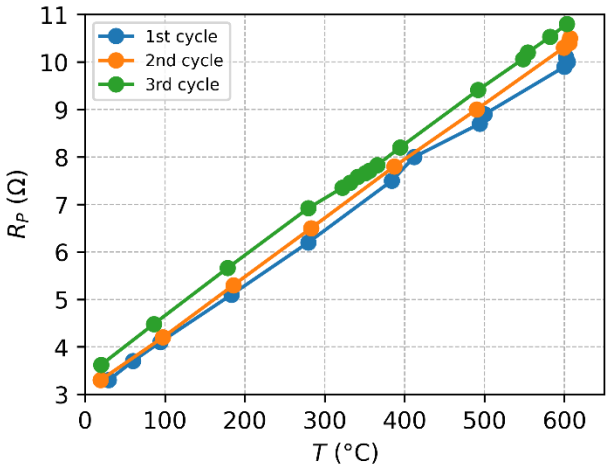
1st cycle
2nd cycle
3rd cycle
$R_P$ (Ω)
$T$ (°C)
11
10
9
8
7
6
5
4
3
0
100
200
300
400
500
600

Fig. 5

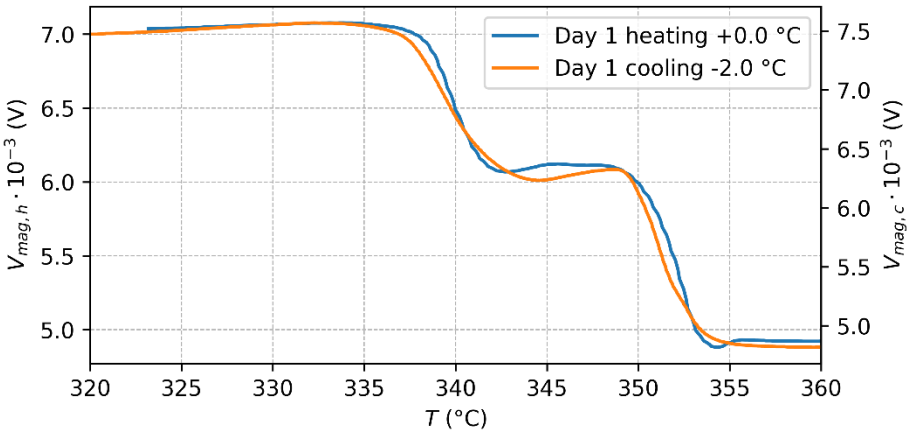
Day 1 heating +0.0 °C
Day 1 cooling -2.0 °C
$V_{mag,h} \cdot 10^{-3}$ (V)
$V_{mag,c} \cdot 10^{-3}$ (V)
$T$ (°C)
7.0
6.5
6.0
5.5
5.0
7.5
320
325
330
335
340
345
350
355
360

Fig. 6

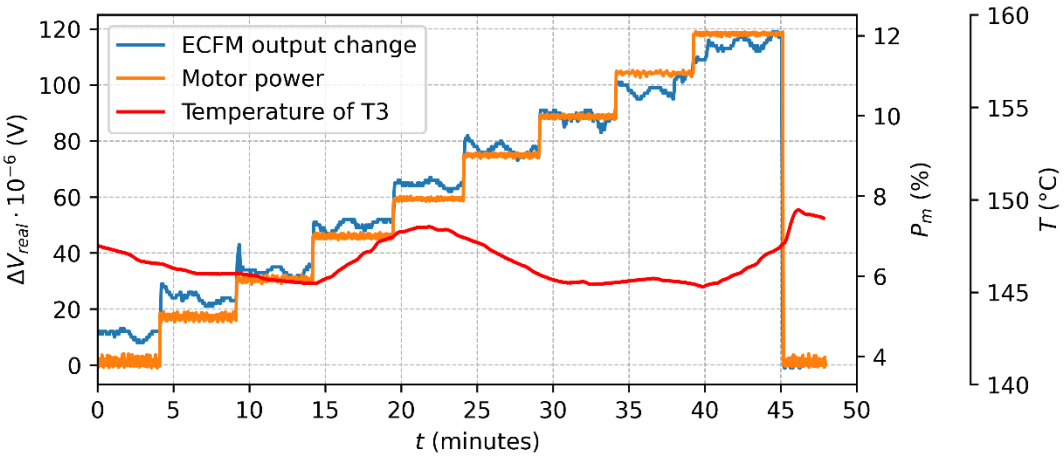
ECFM output change
Motor power
Temperature of T3
$\Delta V_{real} \cdot 10^{-6}$ (V)
$P_m$ (%)
$T$ (°C)
$t$ (minutes)
0
20
40
60
80
100
120
4
6
8
10
12
140
145
150
155
160
0
5
10
15
20
25
30
35
40
45
50

Fig. 7

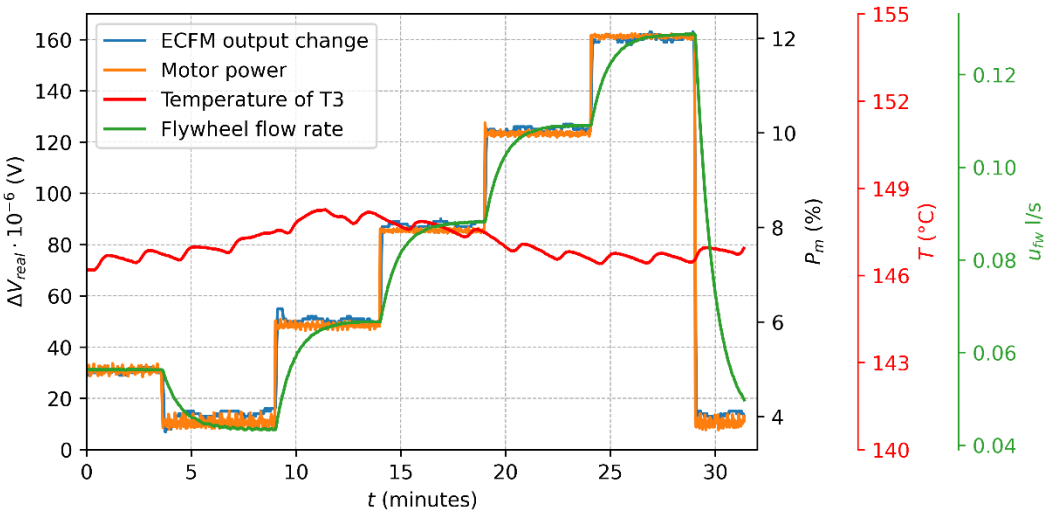
ECFM output change
Motor power
Temperature of T3
Flywheel flow rate
$\Delta V_{real} \cdot 10^{-6}$ (V)
$P_m$ (%)
$T$ (°C)
$u_{fw}$ l/s
$t$ (minutes)

Fig. 8

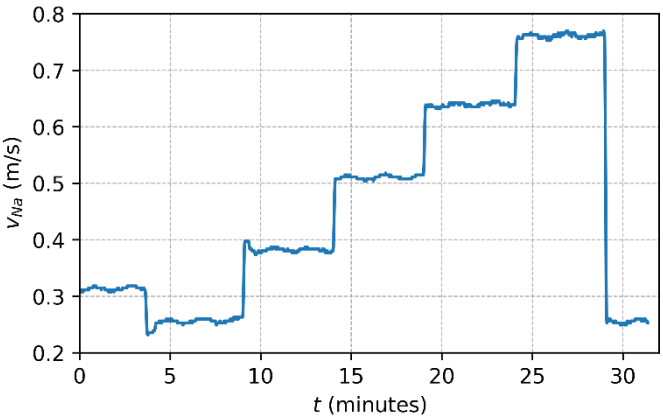


Fig. 9

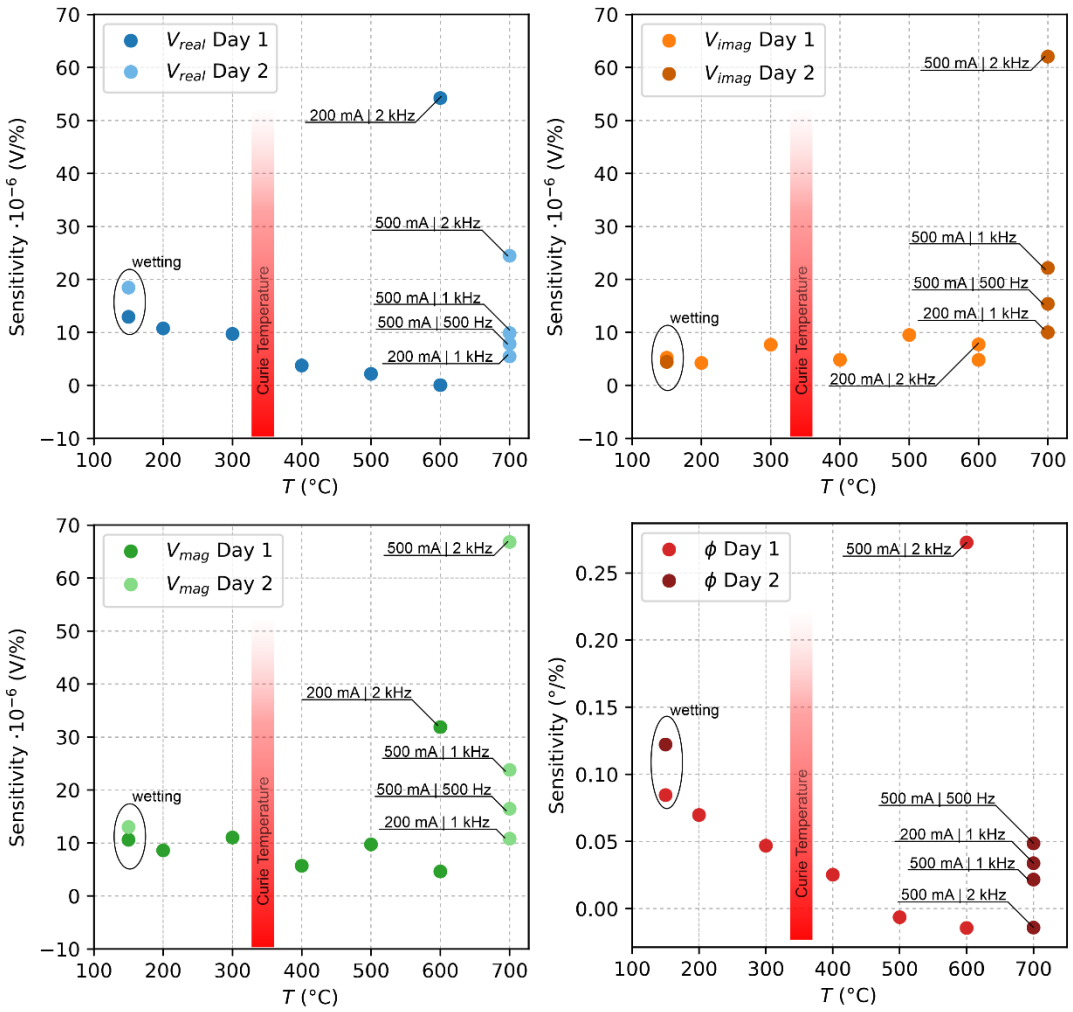
$V_{real}$ Day 1
$V_{real}$ Day 2
$V_{imag}$ Day 1
$V_{imag}$ Day 2
$V_{mag}$ Day 1
$V_{mag}$ Day 2
$\phi$ Day 1
$\phi$ Day 2
Sensitivity ·10⁻⁶ (V/%)
Sensitivity (°/%)
T (°C)
wetting
Curie Temperature
200 mA | 2 kHz
500 mA | 2 kHz
500 mA | 1 kHz
500 mA | 500 Hz
200 mA | 1 kHz

Fig. 10

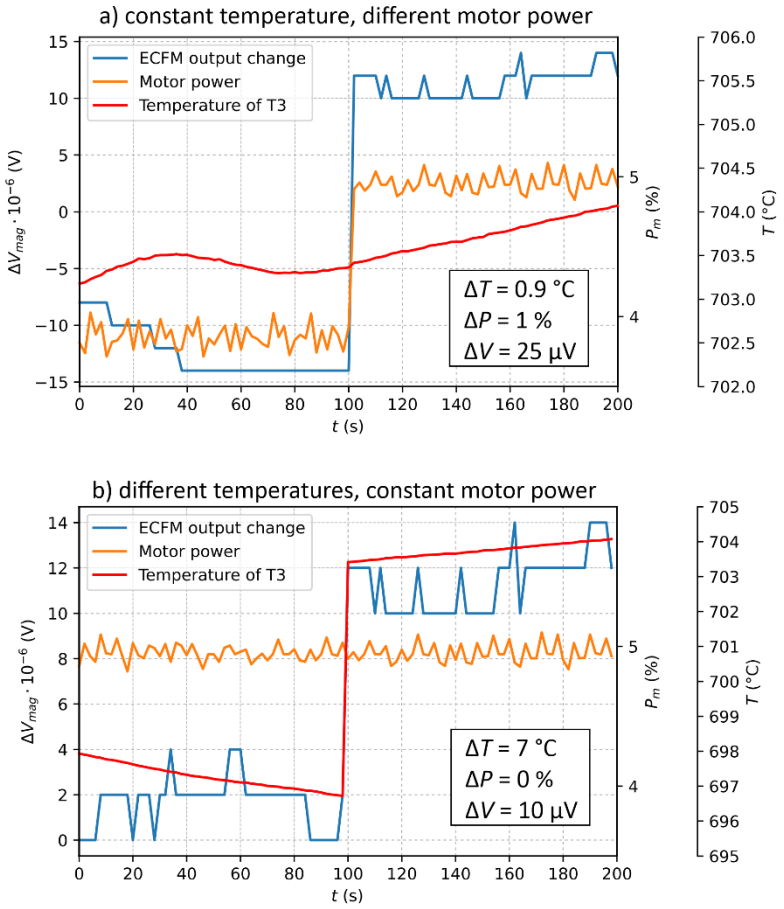
a) constant temperature, different motor power
ECFM output change
Motor power
Temperature of T3
ΔT = 0.9 °C
ΔP = 1 %
ΔV = 25 μV
ΔV_mag · 10⁻⁶ (V)
P_m (%)
T (°C)
t (s)
b) different temperatures, constant motor power
ECFM output change
Motor power
Temperature of T3
ΔT = 7 °C
ΔP = 0 %
ΔV = 10 μV
ΔV_mag · 10⁻⁶ (V)
P_m (%)
T (°C)
t (s)

Fig. 11

Table 1

| T (°C) | Data Points | Real part $s_{rel}$ (%) | Imaginary part $s_{rel}$ (%) | Magnitude $s_{rel}$ (%) | Phase $s_{rel}$ (%) |
|---|---|---|---|---|---|
| 150 (Day 1) | 9 | 1.70 | 14.01 | 5.56 | 5.88 |
| 200 (Day 1) | 4 | 1.67 | 2.36 | 2.21 | 1.43 |
| 300 (Day 1) | 4 | 1.13 | 21.64 | 13.77 | 12.77 |
| 400 (Day 1) | 4 | 6.93 | 17.36 | 13.13 | 24.0 |
| 500 (Day 1) | 3 | 18.43 | 7.04 | 5.65 | 100.0 |
| 150 (Day 2) | 6 | 0.60 | 22.52 | 6.53 | 4.10 |